Simulation of temperature extremes over West Africa with MPAS

Laouali Ibrahim Tanimoune, Gerhard Smiatek, Harald Kunstmann, Babatunde J. Abiodun

Angaben zur Veröffentlichung / Publication details:

Tanimoune, Laouali Ibrahim, Gerhard Smiatek, Harald Kunstmann, and Babatunde J. Abiodun. 2023. "Simulation of temperature extremes over West Africa with MPAS." *Journal of Geophysical Research: Atmospheres* 128 (23): e2023JD039055. https://doi.org/10.1029/2023jd039055.

JGR Atmospheres

RESEARCH ARTICLE
10.1029/2023JD039055

Simulation of Temperature Extremes Over West Africa With MPAS

Laouali Ibrahim Tanimoune[1,2], Gerhard Smiatek[2], Harald Kunstmann[2,3], and Babatunde J. Abiodun[4]

[1]Department of Meteorology and Climate Science, Federal University of Technology of Akure, Akure, Nigeria, [2]Institute of Meteorology and Climate Research (IMK-IFU), Karlsruhe Institute of Technology, Garmisch-Partenkirchen, Germany, [3]Institute of Geography, University of Augsburg, Augsburg, Germany, [4]Department of Environmental and Geographical Science, University of Cape Town, Cape Town, South Africa

Key Points:

- Multiple Model for Prediction Across Scales (MPAS) runs with SST and sea ice extent as the only boundary condition are used to investigate extremes of temperature and heat waves
- MPAS reveals moderate cold biases for all investigated temperature indices
- Long term runs as well as short term runs with selected SST years yield similar results

Correspondence to:
H. Kunstmann,
harald.kunstmann@kit.edu

Citation:
Tanimoune, L. I., Smiatek, G., Kunstmann, H., & Abiodun, B. J. (2023). Simulation of temperature extremes over West Africa with MPAS. *Journal of Geophysical Research: Atmospheres*, *128*, e2023JD039055. https://doi.org/10.1029/2023JD039055

Received 12 APR 2023
Accepted 17 NOV 2023

Abstract A large ensemble of 51 simulations with the Model for Prediction Across Scales (MPAS) has been applied to assess its ability to reproduce extreme temperatures and heat waves in the area of West Africa. With its global approach the model avoids transition errors influencing the performance of limited area climate models. The MPAS simulations were driven with sea surface temperature (SST) and sea ice extent as the only boundary condition. The results reveal moderate cold biases in the range from −0.6° to −0.9°C for the daily mean temperature and −1.2° to −2.0°C for the area mean of the daily maximum temperature. The bias in the number of tropical nights ranges from +3 to −10 days. An underestimation by up to 50% is also present regarding the number of summer days. The heat wave duration index is underestimated regionally by 10%–60%. MPAS simulations are generally closer to the reanalysis results than they are to the observational reference. The results from long term runs and from short term runs with selected SST years are similar. Shortcomings in the reproduction of the temperature and precipitation indices found in the present investigation indicate that the global MPAS approach does provide a fidelity similar to that of the regional climate models.

Plain Language Summary A large number of simulations with the global weather and climate model Model for Prediction Across Scales (MPAS) has been applied to investigate extreme temperatures and related heat waves. The considered area is West Africa. In the simulations sea surface temperature and sea ice extent were the only boundary condition. The results reveal moderate underestimation in the range from −0.6° to −0.9°C for the daily mean temperature. The bias of the area mean of the daily maximum temperature was −1.2° to −2.0°C. An underestimation by up to 50% is also present in the number of summer days. The heat wave duration index is underestimated regionally by 10%–60%. Obtained results in the reproduction of the observed temperatures and precipitation show that the global MPAS model provides results similar to that of regional climate models.

1. Introduction

West Africa (WA) and the Eastern Sahel are characterized by high temperatures and large variability in rainfall (Nicholson & Webster, 2007; Poan et al., 2016; Sultan et al., 2013) and have been historically affected by extreme weather anomalies. A long-standing example is the droughts of 1974–1975 over the Sahel. They caused severe increases in mortality in the population and livestock, and despite the recent occurrence of a regreening, the Sahel region is still suffering from these droughts (Cook, 2008; Janicot et al., 1996).

Several studies have provided evidence for a considerable warming in West Africa and the Sahel in the recent past. New et al. (2006) showed that most stations in West Africa reveal positive trends in the minimum and maximum temperature over the period 1961–2000. That study also found increases in both the number of hot days and of cold days. Evaluating reanalyses and CORDEX models, Adeniyi and Oyekola (2017) found that the magnitude of the frequencies of heat waves in West Africa has increased. Oueslati et al. (2017) found that heat waves are spatially increasing with high intensity. Similar findings are reported concerning increases in temperatures and the frequencies of heat waves, particularly in the Sahel (Dosio, 2017; Ringard et al., 2016; Russo et al., 2016). Further increases are projected for the future. From results based on CMIP5 model simulations, Ringard et al. (2016) reported significant increases in heat waves for the Sahel in all applied scenarios.

Table 1
Parametrization Schemes Used by the Simulations

Parametrization	Scheme
Convection	New Tiedtke
Microphysics	WSM6
Land surface	Noah-LSM
Boundary layer	YSU
Surface layer	Monin–Obukhov
Radiation, LW	RRTMG
Radiation, SW	RRTMG
Cloud fraction for radiation	Xu–Randall
Gravity wave drag by orography	YSU

An increase in the severity and frequency of heat wave events can lead to the loss of human lives and the destruction of crops. Extreme temperatures and heat waves strongly affect the socio-economic conditions in various sectors, such as agriculture, infrastructure, and energy (Coumou & Rahmstorf, 2012; Lobell et al., 2011; Perkins et al., 2015). A weak economy, an inefficient policy, and a limited resilience increase the vulnerability. Hence, modeling tools capable of simulating extreme present and expected future climate conditions have gained increasing importance for the support of policymakers.

The scientific aim of this study is the evaluation of the global Model for Prediction Across Scales (MPAS), driven with sea surface temperature (SST) and sea ice extent as the only boundary condition, with regard to its ability to simulate extreme temperatures and heat waves in West Africa and the Eastern Sahel. In addition, basic precipitation indices are investigated. With its global approach, the model prevents the errors commonly introduced in regional climate models (RCMs) in the transition zone from the driving GCM (General Circulation Model) to the regional model, and thus provides an additional tool applicable to the vital questions related to present and future climate conditions. Dosio et al. (2022) points out that RCMs do not improve the simulation ability of large-scale fields compared to GCMs.

So far, MPAS has only been applied to this region by Heinzeller et al. (2016), who had a focus on the reproduction of the dynamics of the West African monsoon (WAM) and the associated precipitation.

Unlike RCM applications, global MPAS runs are not confined by a driving model but, besides the boundary conditions, depend on their initialization. Thus, an additional aim of this study is the comparison of two different initialization procedures.

This study considers the summer season as the most important period for the regional economy, which greatly relies on agriculture, which depends on the seasonal rainfall and the behavior of the monsoon rains (Sivakumar et al., 2014) and is generally practiced during the summer. Any changes during this crucial period often have a devastating effect on socio-economic activities and food security in the region (Dilley & Heyman, 1995; Haile, 2005; Omotosho & Abiodun, 2007). Drought, excessive rains, or heatwaves during the growing season can potentially diminish crop yield, especially in the Sahel, where water is a particularly determining element for the growth of the crops (Ahmed et al., 2015).

The present study is structured as follows: Section 2 describes the applied model, reference data, investigation areas and the evaluation indices. The results of the evaluation are presented and discussed in Section 3, and conclusions are drawn in Section 4.

2. Material and Methods

2.1. MPAS Model

The applied meteorological model is the Model for Prediction Across Scales (MPAS), which is based on unstructured Voronoi meshes and C-grid discretization (Ringler et al., 2010; Thuburn et al., 2009). MPAS-atmosphere (Skamarock et al., 2012), used in the present study, is a global, fully compressible non-hydrostatic model (Klemp, 2011). The model is run at an approximately 60-km resolution mesh with a total of 163,842 cells, applying the mesoscale reference physics suite, 55 vertical levels up to a height of 30 km, and four soil levels. The land–surface physics component is the Community Noah Land Surface Model (Noah-LSM) (Chen et al., 1996).

Table 1 shows the associated parametrization schemes of the standard model configuration. These are tested and recommended parameterizations suitable for mesoscale resolutions larger than 10 km. MPAS provides a different set of parameterizations schemes for convection-permitting meshes with a resolution below 10 km. Potential uncertainty might be related to the in MPAS only available Noah LSM. Glotfelty et al. (2021) found with this LSM larger cold and dry biases in sub-Sahaian Africa. The RRTMG (Clough et al., 2005) long-wave and short-wave radiation scheme uses a fixed value for carbon dioxide, reflecting the conditions of the years around 2004. The static input fields applied are the MODIS 20-class land cover based on global land cover climatology collected in 2001–2010 at 500-m resolution (Broxton et al., 2014) and the Global Multi-Resolution Terrain

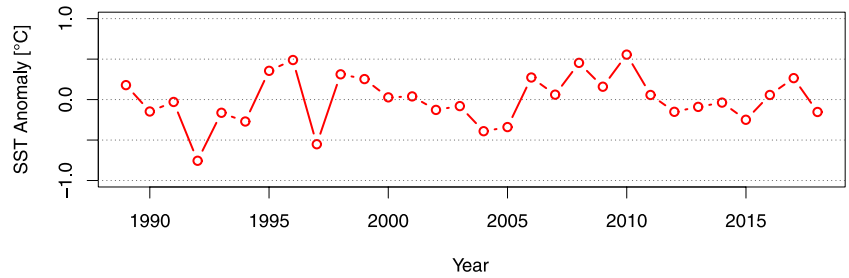

Figure 1. SST anomaly over the Gulf of Guinea as in ERA-Interim 1989–2018.

Elevation Data (GMTED2010) (Danielson & Gesch, 2011) topography. The surface albedo and vegetation fraction are updated monthly from MODIS climatology.

2.2. Performed Simulations

An MPAS simulation with SST and sea ice extent as the only boundary condition does not reproduce the weather of a specific year, but it creates weather patterns that fit these conditions. Thus, in order to reproduce the observed climatology, multiple runs with different initialization dates are required. The present article presents 51 MPAS simulations. They form three experiments, denoted by MPAS_A, MPAS_B and MPAS. Experiment MPAS_A applies the initialization data, SST and sea ice extent from the ERA-Interim reanalysis (Dee et al., 2011) and follows the procedure applied by Smiatek and Kunstmann (2023). Six years have been selected according to the SST anomaly in the Gulf of Guinea during the summer season (Figure 1). The Gulf of Guinea has a central influence on the precipitation in West Africa (Son & Seo, 2020). The considered period covers 30 years around 2004, from 1990 to 2019. Specific years are 1992 and 1997, revealing a negative anomaly, 1998 and 2010 with a positive anomaly, and 2003 and 2016 are neutral. These anomalies basically correspond to positive and negative ENSO states. Within each SST–year, five simulations initialized from May 15 through May 19 and run until September 1 have been performed.

Experiment MPAS_B is a continuous MPAS simulation initialized in December 1980, from which the results for the period 1990–2010 are applied in the present investigation. For the initialization, the SST and sea ice extent data from the Climate Forecast System Reanalysis (CFSR) (Saha et al., 2014) are used. CFSR data is available until 2010. The chosen period covers the largest SST anomalies in the Gulf of Guinea (Figure 1).

The MPAS experiment consists of MPAS_A and MPAS_B simulations lumped into a single ensemble. The investigated period is the summer season (JJA).

2.3. Observational Reference and Investigated Areas

The present investigation uses a set of available gridded temperature and precipitation reference data at monthly and daily resolution. These are interpolated station and gauge measurements (CPC, CRU), extended satellite measurements (CHIRTS and CHIRPS, together CHIRPS/TS), as well as state of the art reanalyses (ERA5, JRA-55, MERRA-2, NCEP-2). Table 2 provides some details about the applied data. With the exception of the CHIRTS data, which is available only up to 2016, all data sets cover the investigated period, 1990–2019. CRU only provides monthly resolution and therefore is used only in the basic statistics.

The results of the performed simulations are analyzed in two areas in the Sahel region, SAH_W (Sahel-West) and SAH_E (Sahel-East), and one area at the coast of Guinea, GUI_C (Guinea-Center), as well as for the entire region. There are no standard evaluation areas available so far for West Africa and the Sahel. However, the areas SAH_W and SAH_E have been used by several studies (Dosio, Jury, et al., 2021; Dosio, Pinto, et al., 2021; Smiatek & Kunstmann, 2023), and thus allow putting the results in the context of previous investigations. Figure 2 shows the MPAS 60-km mesh and the investigation areas.

2.4. Investigated Indices

The investigated temperature related indices were selected from the perspective of the socio-economic activities in the investigated region and comprise indices used by similar investigations (Engdaw et al., 2022), mostly

Table 2
Reference Data Applied in the Present Study

Acronym	Name	Resolution	Type	Reference
ERA5	ECMWF ERA5	0.25°	R	Hersbach et al. (2020)
JRA-55	Japanese 55-year Reanalysis	1.25°	R	Kobayashi and Iwasaki (2016)
MERRA-2	Modern-Era Retrospective Analysis for Research and Application, v. 2	0.5 × 0.625°	R	Gelaro et al. (2017)
NCEP-2	NCEP-DOE Reanalysis 2	1.875°	R	Kanamitsu et al. (2002)
CHIRTS	Climate Hazard Group Infrared Temperature with Stations	0.25°	M,S,R	Funk et al. (2019)
CHIRPS	Climate Hazard Group InfraRed Precipitation with Station Data	0.25°	G,S	Funk et al. (2015)
CPC	CPC Global Unified Temperature	0.5°	G	NOAA PSL, Boulder
CRU	Climate Research Unit	0.5°	G,M	Harris et al. (2020)

Note. G denotes the gauge, M, the monitoring station, R, reanalysis, and S, satellite measurements.

defined by the Expert Team on Climate Change Detection, Monitoring and Indices (ETCCDI) (Karl et al., 1999) with adjusted thresholds. They are the daily mean (TG), minimum (TN) and maximum (TX) temperature, the number of tropical nights (TR) with TN > 24°, the percentage of warm nights (TN90p) with TN > 90th percentile, the number of summer days (SU) with TX > 35°, the percentage of warm days (TX90p) with TX > the 90th percentile, and the heat wave duration index (HWDI) with TX > TXnorm +3°over at least three days. TXnorm is calculated as the mean of the maximum temperatures of a five-day window over all simulations and with the reference data from the entire investigated period.

The indices related to precipitation are the daily mean precipitation (RR), the number of wet days (RR1), and the maximal daily rainfall (RX1day). These indices allow a comparison with the investigation of the observed and simulated precipitation characteristics provided by Dosio, Jury, et al. (2021) and Dosio, Pinto, et al. (2021).

Table 3 shows the indices, their definitions, and their units. All indices are calculated for land points only and were derived from instantaneous 3-hourly MPAS output for MAPS_A and 1-hourly output for MAPS_B. An investigation of the impact of the output frequency in comparison with an 1-hourly output was performed for the JJA season and the year 2016. The results reveal that in average the 3-hourly output underestimates the daily maximum temperature TX by −0.2°C. The mean value TG is not influenced by the investigated output frequency.

3. Results

Figure 3 shows the distributions of the area mean summer (JJA) mean temperature TG in the investigated areas SAH_W, SAH_E and GUI_C for both the reference data and the MPAS simulations. It reveals that the results obtained from MPAS are well within range, and there are only small differences between the different simulation approaches of MPAS_A and MPAS_B.

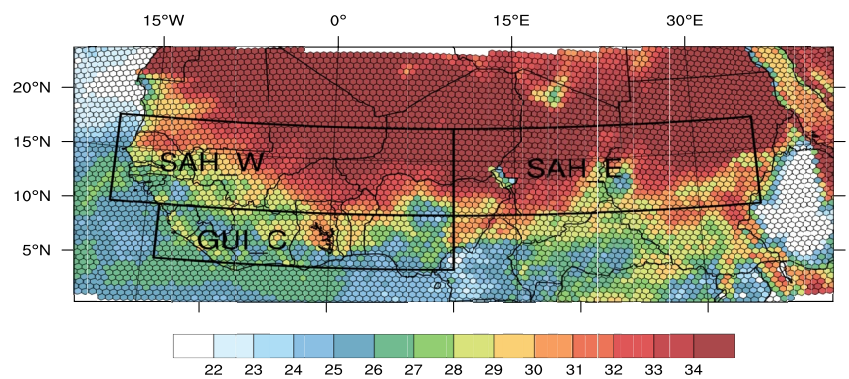

Figure 2. MPAS 60 mesh and investigated areas SAH_W, SAH_E, and GUI_C. Simulated 2-m temperature (01.07.2010:12:00 UTC).

Table 3
List of Indices Analyzed in This Study

Index	Definition	Units
TG	Seasonal mean of daily mean temperature	°C
TN	Seasonal mean of daily minimum temperature	°C
TX	Seasonal mean of daily maximum temperature	°C
TXx	Seasonal maximum of TX	°C
TR	Number of tropical nights with TN > 24°	d
TN90p	Percentage of days when TN > 90th percentile	%
SU	Number of summer days with TX > 35°	d
TX90p	Percentage of days when TX > 90th percentile	%
HWDI	Heat wave duration index. TX > TXnorm + 3° over at least 3 days	d
RR	Daily mean precipitation	mm/d
RR1	Number of wet days when RR ≥ 1 mm	d
RX1day	Maximal daily RR	mm/d

Note. The indices are calculated on a seasonal (JJA) basis.

Concerning the ranges and the area mean value, there are substantial differences in the reference data (Table 4). In the SAH_W area, the mean value TG in the reanalyses extends from 28.4°C to 29.4°C, the range in the data based on observations is from 29.5°C to 29.9°C. MPAS shows, with 28.7°C, a cold bias of −0.6°C in relation to the mean of the entirety of the reference data, of −0.4°C in relation to the mean value of the reanalysis products, and −1.1°C to the observational reference. The corresponding biases in the SAH_W area are −0.6°, −0.3°, −1.2°C, and in the GUI_C area, −0.9°, −0.5°, and −1.6°C.

These results are comparable to the findings from previous simulation experiments. For instance, Hernández-Díaz et al. (2013) found, over West Africa, biases in the simulations with the Canadian Regional Climate Model (CRCM5) in the range from −2°C to 2°C. Gbobaniyi et al. (2014) found, with the WRF model, biases of 0.8°C over West Africa, of 0.8°C over Guinea, and 1.6°C over the Sahel during the JAS (July, August, September) period. With the RCA4 model, Nikiema et al. (2017) reported biases of 1.2°C over WA, 1°C over Guinea and

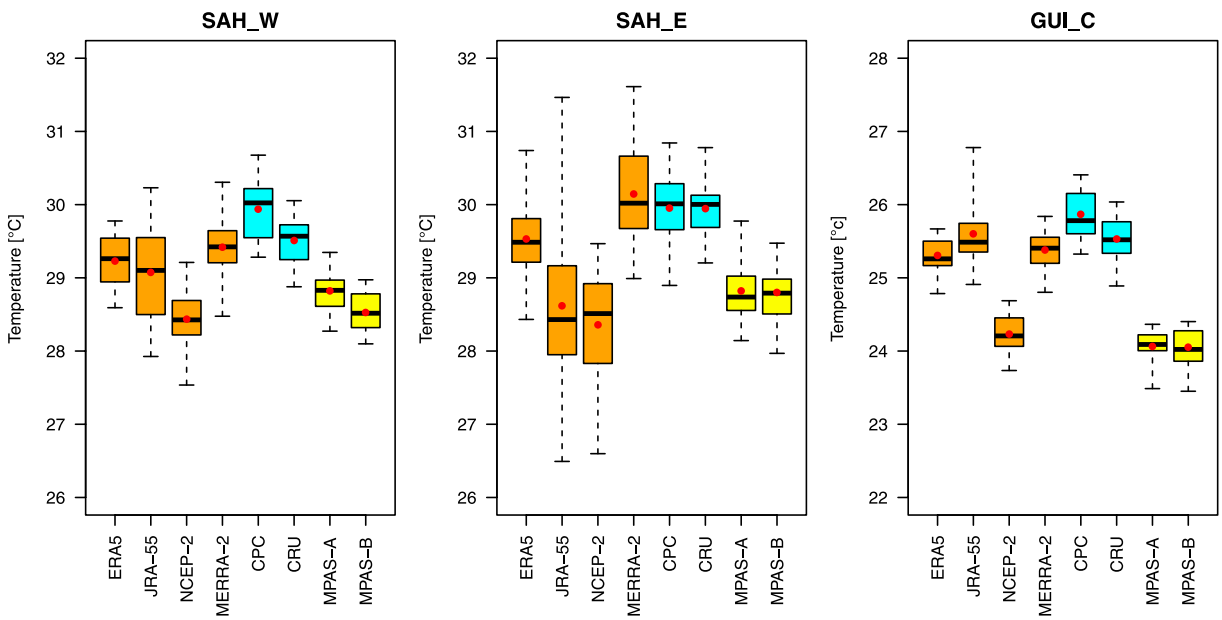

Figure 3. Boxplots of the area mean summer (JJA) mean temperature TG in the investigated areas SAH_W, SAH_E and GUI_C.

Table 4
Mean Values of Temperature Indices Over the Investigation Areas for the JJA Season, Both Observed and Simulated

Area	Data	TG (°C)	TX (°C)	TXx (°C)	TR (d)	SU (d)	TN90p (%)	TX90p (%)	HWDI (d)
SAH_W	ERA5	29.2	34.3	40.3	51.7	41.1	14.2	20.1	10.7
	JRA-55	29.1	33.2	40.5	52.5	31.1	29.9	34.3	40.9
	NCEP-2	28.4	32.4	40.5	50.2	29.8	5.3	57.5	34.4
	MERRA-2	29.4	34.7	41.3	49.0	41.9	15.1	20.2	18.5
	CPC	29.9	34.5	41.2	58.7	40.7	15.5	15.6	18.6
	CRU	29.5	35.0	–	–	–	–	–	–
	CHIRTS	–	34.9	40.9	68.6	42.5	17.6	17.6	5.5
	MPAS_A	28.8	33.1	38.5	52.3	33.6	13.8	11.5	8.5
	MPAS_B	28.5	32.7	38.6	49.5	31.7	8.1	14.7	6.3
	MPAS	28.7	32.9	38.6	50.9	32.7	11.0	13.1	7.4
SAH_E	ERA5	29.5	34.9	40.4	46.4	49.0	21.0	27.3	14.3
	JRA-55	28.6	32.9	39.4	39.4	34.8	46.9	54.1	40.6
	NCEP-2	28.4	32.7	40.7	41.3	33.9	17.2	76.4	55.1
	MERRA-2	30.1	36.0	41.6	48.2	54.7	26.7	32.5	23.5
	CPC	30.0	35.3	42.0	52.8	47.7	26.9	20.7	24.9
	CRU	29.9	36.4	–	–	–	–	–	–
	CHIRTS	–	37.1	42.6	78.5	61.5	28.7	28.7	8.6
	MPAS_A	28.8	33.2	38.7	51.8	33.6	25.2	22.1	18.1
	MPAS_B	28.8	32.8	38.2	56.4	29.7	19.8	21.7	10.1
	MPAS	28.8	33.0	38.5	54.1	31.7	22.5	21.9	14.1
GUI_C	ERA5	23.3	28.5	31.9	5.8	0.2	8.4	15.0	0.4
	JRA-55	25.6	28.5	32.3	14.7	1.9	13.1	18.0	9.7
	NCEP-2	24.2	25.9	32.1	8.1	0.1	4.2	55.1	9.1
	MERRA-2	25.4	28.7	32.3	5.0	0.8	9.2	19.7	8.3
	CPC	25.9	29.0	33.4	19.2	0.2	15.6	19.3	7.7
	CRU	25.5	29.2	–	–	–	–	–	–
	CHIRTS	–	29.7	33.4	26.0	0.2	15.6	15.6	0.2
	MPAS_A	24.1	27.4	30.6	3.1	0.0	12.2	15.5	1.1
	MPAS_B	24.1	26.8	30.1	2.0	0.0	11.4	10.3	0.5
	MPAS	24.1	27.1	30.4	2.6	0.0	11.8	12.9	0.8

1.2°C over the Sahel. Kim et al. (2014) concluded from the CORDEX-Africa experiment with 10 regional climate models, seasonal (JJAS) biases ranging from −0.5°C to 0.8°C over West Africa. Dosio et al. (2015) found in simulations with the COSMO-CLM model cold biases up to 3°C in the Guinea region and the southern Sahel. Careto et al. (2018) reported in CORDEX-Africa experiments cold biases in most of Africa for all RCMs, with the largest biases over the Sahel. With the MPAS model, Maoyi and Abiodun (2021) found a cold bias up to 2°C over the Indian Ocean and cold biases up to 1.2°C within the southern African countries. They attributed the error primarily to the coarser resolution of 240 km applied in the simulations and to the fact how MPAS resolved the topography over high elevation areas in Botswana, Angola, Zambia and western parts of Tanzania.

Figures 4–5 depict boxplots of the mean daily maximum temperatures TX and TXx, for the reference data and the MPAS simulations. The corresponding area mean values are shown in Table 4. Compared to the mean values, the cold biases are larger. In the SAH_W area, a cold bias of −1.2°C compared to the mean of all the reference data is present for TX. It is −2.2°C for TXx. The cold biases related to the reanalyses are smaller. However, it has be taken into account that NCEP-2 and JRA-55 have a much lower resolution and are generally cooler than ERA5 and MERRA-2. Related to the observations, the MPAS cold biases are larger, at −2.1°C and −2.5°C, respectively.

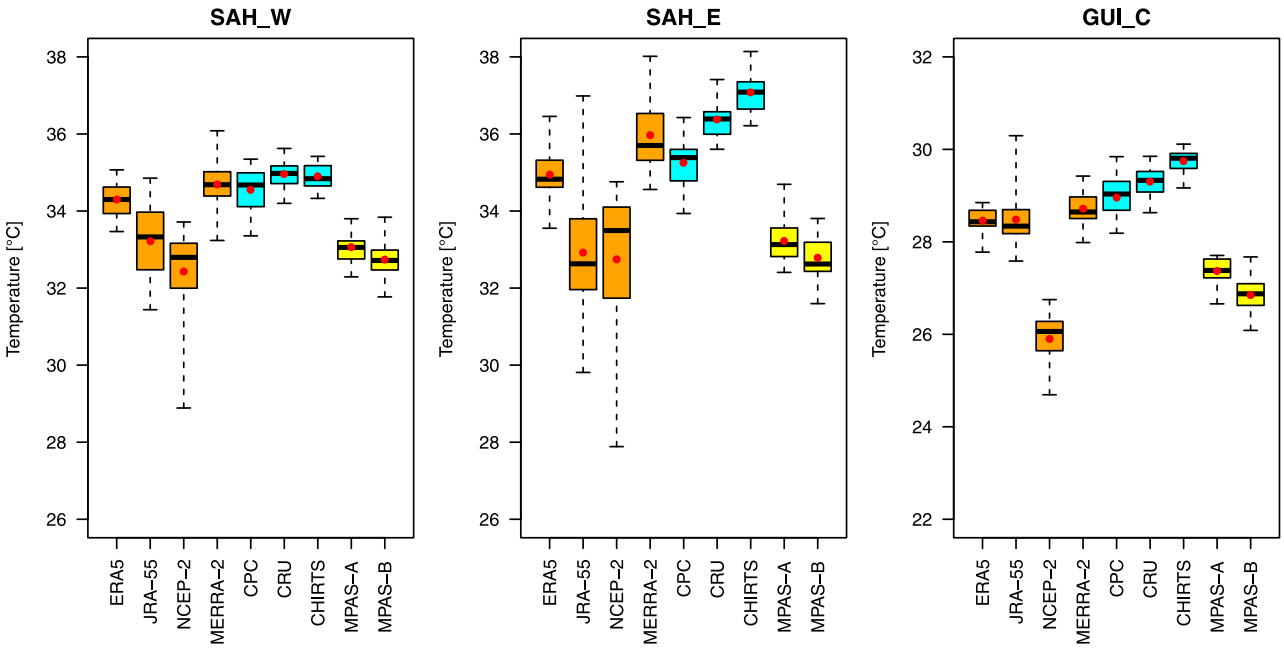

Figure 4. Boxplots of mean daily maximum temperature TX for the reference data and MPAS simulation in the investigation areas SAH_W, SAH_E, and GUI_C and the summer season (JJA).

The results obtained for the SAH_E and GUI_C areas are similar. However, the biases are larger when only the observational reference is considered. In general, there are large differences between the reanalysis data. Especially, the coarsely resolved NCEP-2 and JRA-55 show extremely wide distributions.

The estimated number of tropical nights TR is, in SAH_W and SAH_E, within the range of the reference data (Figure 6) and only in the GUI_C area there is a larger bias of −10 days (−80%) present. When compared to observations only, biases ranging from −12 to −20 days are present. The number of tropical nights and its range

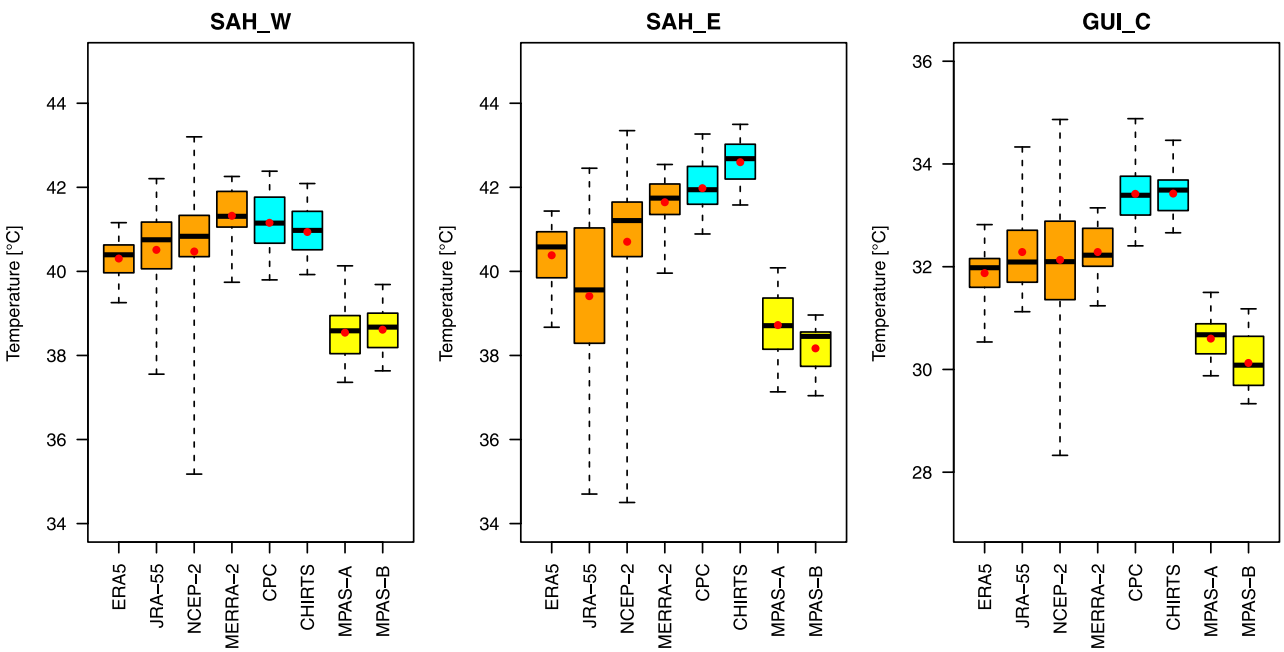

Figure 5. Boxplots of maximum daily maximum temperature TXx for the reference data and MPAS simulation in the investigation areas SAH_W, SAH_E, and GUI_C and the summer season (JJA).

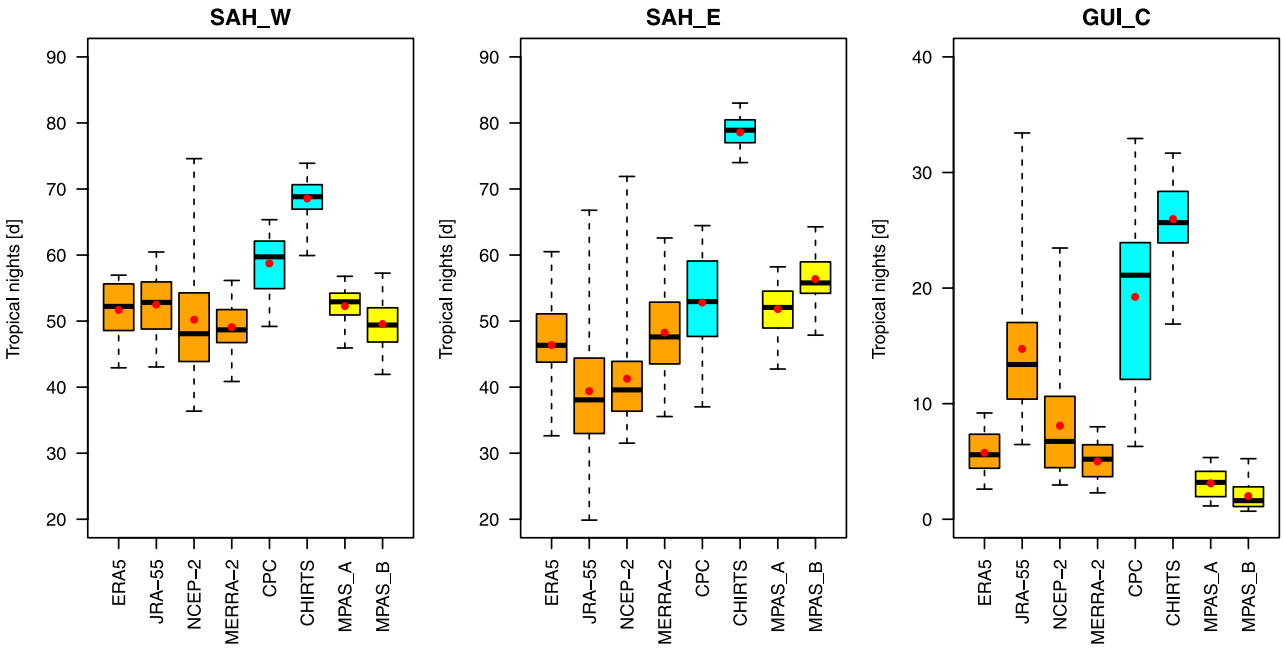

Figure 6. Boxplots of the number of tropical nights TR with daily minimum temperature over 24°C for the reference data and MPAS simulations in the investigation areas SAH_W, SAH_E, and GUI_C and the summer season (JJA).

in the GUI_C area is comparatively small, but it is similar to the range of the reanalyses ERA5 and MERRA-2. CHIRTS reveals in all areas the highest minimum temperatures and thus a high number of tropical nights.

The same findings apply to the number of summer days SU (Figure 7), where this number is slightly underestimated, by 5 days (14%) in the area SAH_W and by 15 days (33%) in SAH_E. The number of summer days in the GUI_C area is very small and therefore not considered here.

Biases in the percentiles TN90p and TX90 reach values of −33% and −53% in SAH_W, −19% and −7% in SAH_E and +7% and −46% in GUI_C when compared to the mean values of the reference data. The biases are larger in SAH_E and GUI_C and smaller in SAH_W when the reference are observations only. Finally, the largest biases, reaching −66% in SAH_W and −86% in GUI_C, are found for the heat wave duration index HWDI. In SAH_E, this bias is, at 10%, rather small.

In summary, it can be concluded that there are moderate to partly large biases in the summer area mean values of the investigated indices. These are in general cold biases and underestimations of the reference data. The biases are larger when only the observational reference is considered. On the other hand, the ranges in the MPAS simulations and in the observations are similar. In relation to the reanalyses this bias is smaller. The reanalyses, especially NCEP-2 but also JRA-55 reveal a cold deviation in comparison with the observation data. Also, these reanalyses show larger ranges, possibly due to the coarser resolution.

MPAS reaches, when biases in percent of the reference are considered, the lowest biases in the SAH_W area in five of the investigated indices. Limiting this comparison to the reference from observations yields the lowest biases in four indices in SAH_E and four in SAH_W. In the complex coastal area GUI_C, MPAS simulations reveal the highest biases. As in the CORDEX-experiments (Kim et al., 2014), the biases simulated for West Africa are generally smaller than for the eastern part of the Sahel. This might however be related to the lower density of monitoring stations in this region (Masunaga et al., 2019). Dosio (2017) found, regarding the summer mean temperature (TG), large discrepancies between the individual simulations, with the model spread ranging from 3.5°C over the coast of Guinea, to 7°C, over SAH_E.

Despite the deficiencies, the general applicability of MPAS to climate simulations can be concluded here. Larger biases are found at regional scales.

Figure 8 shows maps of the MPAS simulated mean maximum temperature (TX) and differences between MPAS, as the mean value of the MPAS_A and MPAS_B experiments, and the mean of the applied reference data. In

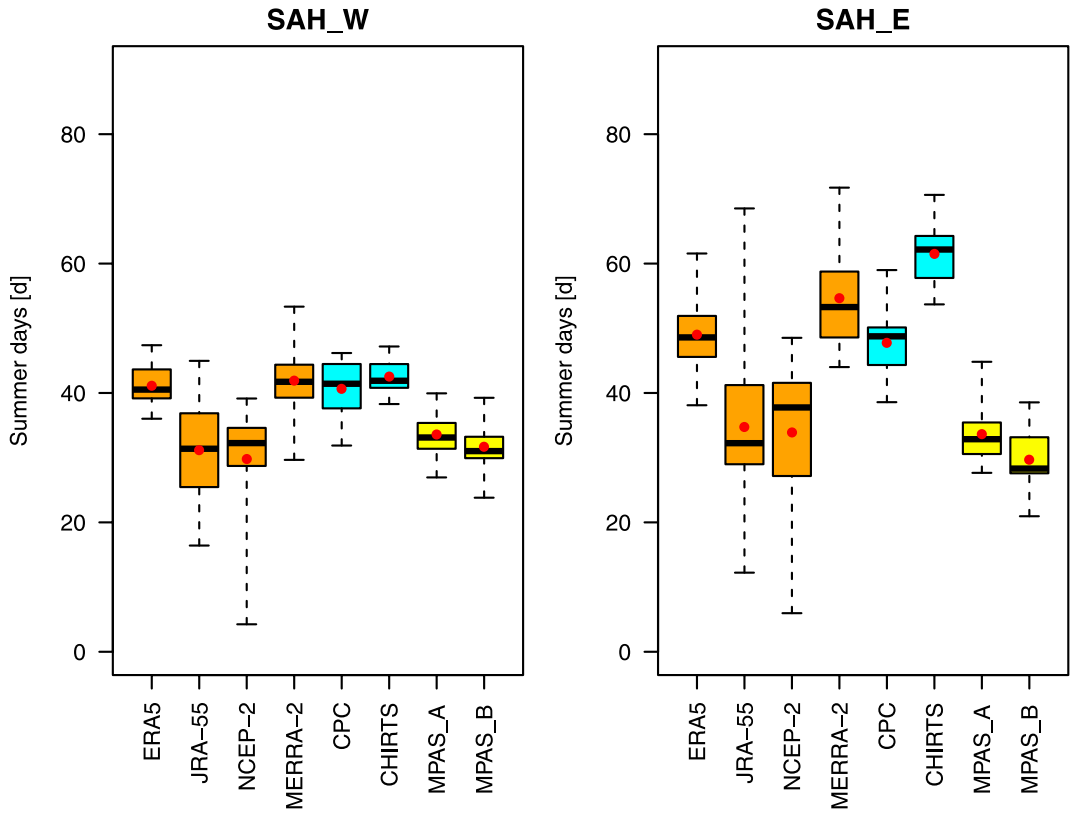

Figure 7. Boxplots of the number of summer days SU with temperature over 35°C for the reference data and MPAS simulations in the investigation areas SAH_W and SAH_E.

comparison, MPAS reveals a notable cold bias throughout the considered region. Only in the Volta region and in the Western Sahara are there small positive biases. In comparison with the reanalyses, the biases are generally smaller, reveal however, similar negative values with MERRA-2 and CHIRTS. The results with JRA-55 and NCEP-2 differ and show also positive biases. The smallest differences occur with the ERA5 reference. Compared to ERA5, MERRA-2 and the observational references MPAS shows systematic negative biases. Taking into account the biases in the observations resulting from the rather low station density in some areas and the coarser resolution of the other reanalysis data, it can be concluded that the MPAS performs reasonably well. However, in relation to the reanalyses, the obtained bias is probably underestimated as the NCEP-2 and JRA-55 reanalyses have only a coarse resolution which averages the extreme temperatures.

The patterns of the differences in the number of summer days (SU) with daily maximum temperature TX > 35°C (Figure 9) are similar in the Sahel, showing large underestimations, especially in the eastern part. Positive biases are found in the hot northern part of the Sahel and Saharan zones, while in WA the biases are rather small. Dosio (2016) argued from the results of the CORDEX-Europe experiment that the underestimation of the number of summer days SU is the consequence of the underestimation of the daily maximum temperature TX. The biases in the southern parts of the investigated area are smaller. However, the number of observed SU days is small there. The distribution of SU days exhibits a distinct north-south boundary. This boundary corresponds to the extent of the summer precipitation belt with lower temperatures and in the result lower number summer days in the JJA season.

The simulated heat wave duration index (HWDI) and the differences between the MPAS and the reference data are shown in Figure 10. The picture here is, however, not clear. While a positive bias dominates in the CHIRTS data, this bias is negative for the CPC observations. The differences from JRA-55 and NCEP-2 are mostly negative. With ERA5 and MERRA-2, positive biases dominate the northern part. In the southern part, the biases are rather negative and larger with the JRA-55 reanalysis. The largest discrepancies seem to occur around the latitude of 15°N.

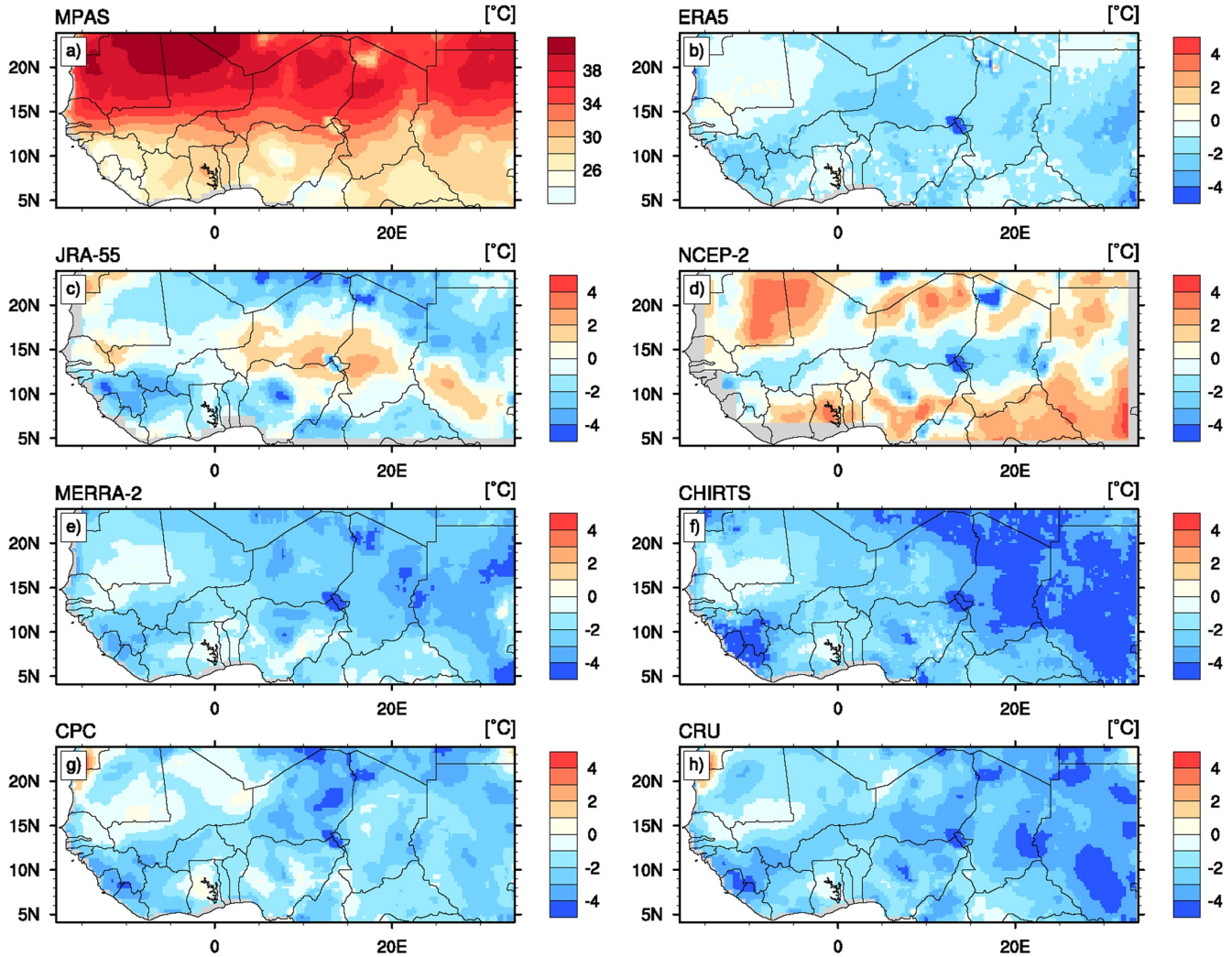

Figure 8. Simulated MPAS mean maximum temperature TX and differences between the MPAS and reference data. For the explanation of the acronyms of the reference data, see Table 2.

Summarizing the regional findings, it can be concluded that a cold bias in the TX is evident. It dominates the results obtained for the related temperature indices. Due to large differences between the single reference data, those results are less clear.

The cold biases in MPAS may contribute to dry biases in the simulated rainfall, as the temperature gradient is the origin of jets which in turn transport moisture and the development of rainfall over the Sahel (Grist & Nicholson, 2001). In addition, the deficiencies in precipitation may also be related to the fact that the MPAS underestimates the number of summer days. SU can affect the convection and regional precipitation recycling (Arnault et al., 2016) over WA and the Sahel. Nicholson and Webster (2007) argued that the reduction in the number of mesoscale convective systems negatively influences the formation of rainfall over the Sahel.

Table 5 and Figure 11 show the results for the investigated precipitation indices in the investigation areas SAH_W and SAH_E in comparison with observational reference from satellite, gauge and reanalysis products as presented by Dosio, Pinto, et al. (2021). It reveals an underestimation of the observed amount of daily precipitation RR in the SAH_W area by 1.6 mm/d or 38%, and is outside the range of the observational data sets. In SAH_E, MPAS slightly overestimates the observations, by 4%, and is well within the range of the reference data. Only small biases are present in the number of rainy wet days (RR1) with precipitation of at least 1 mm in the area SAH_W. It means that the model underestimates the precipitation intensity on such days. The area mean maximum daily rain Rx1day is underestimated on the order of 40%. In SAH_E, RR1 is overestimated by 37% and the maximum

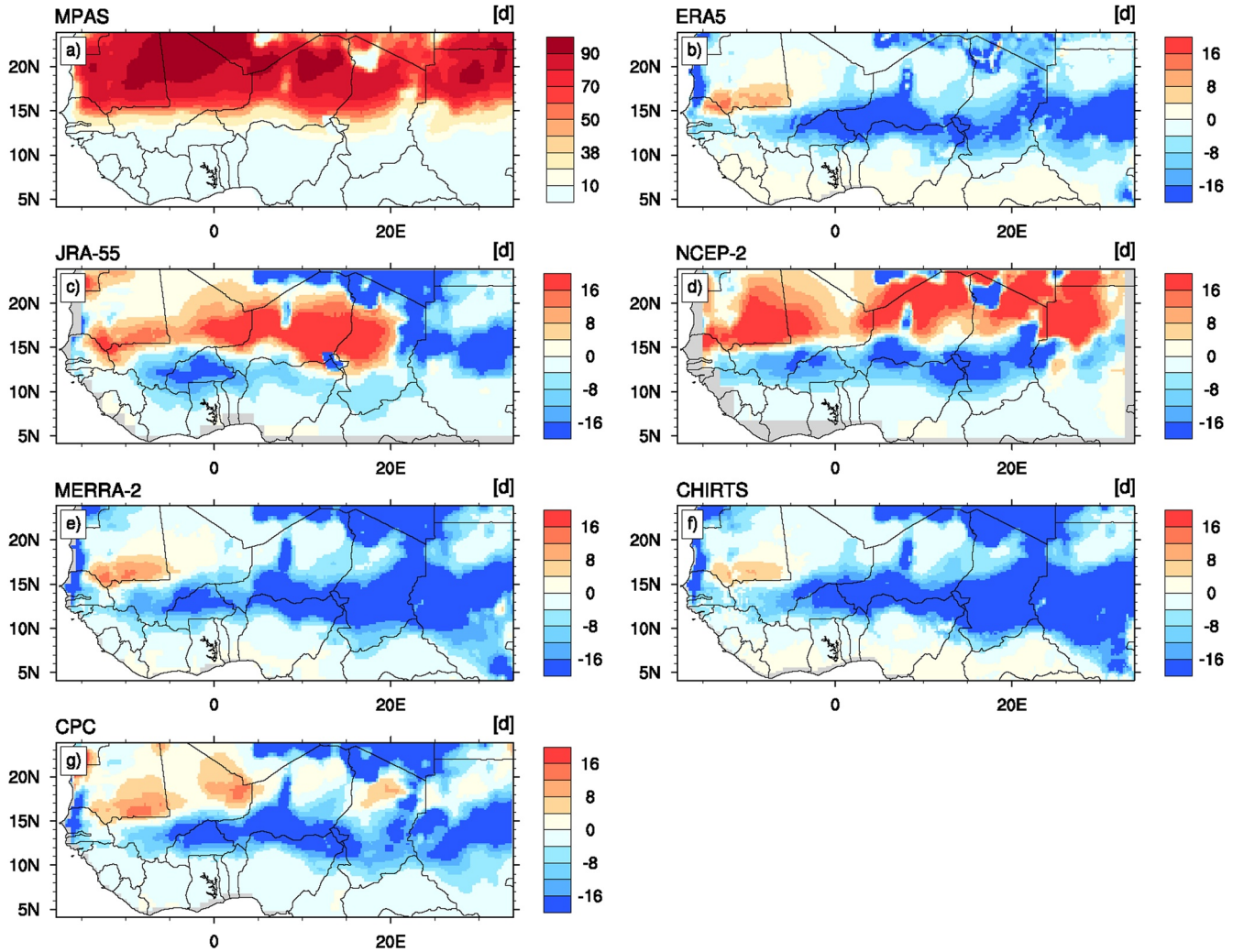

Figure 9. As in Figure 8 but for the number of summer days SU with daily maximum temperature TX > 35°.

daily rain is underestimated by 31%. The investigations of Dosio, Jury, et al. (2021) based on CMIP5, CIMIP6 global models and CORDEX experiments found a large spread between the models. The MPAS results are within the range of those findings. However, it has to be concluded that it has a significant dry bias for West Africa.

Figure 12 shows the mean summer precipitation as in the MPAS simulations, in ERA5 reanalysis and in CHIRPS observations. It reveals dry biases in simulated precipitation in large areas of West Africa. In those areas also a moderate cold temperature bias is present. The mean dry bias in comparison toe the CHIRPS reference is −1 mm/d and to the ERA5 data −0.6 mm/d. Largest dry biases are present in the entire coastal area from Senegal to Cameroon. In the Western Sahel zone and in the eastern part wet biases are present. As there is a cold bias in both TG and TX in the entire area south of the 15°N a rather general deficiency in the model performance can be concluded. In the present MPAS simulations, the cold bias over the Sahel generally weakens the simulated south-west monsoon flow and its inland transport of the moisture. However, due to the direction of the flow, the impacts of reduced moisture on precipitation are more pronounced in Western Sahel with dry biases than over the Eastern Sahel with smaller biases.

Wide range of reasons has been discussed explaining the obvious deficiencies of the climate models in reproducing observed temperature and precipitation characteristics in WA and the Sahel. They are related to a misplacement of the center of the monsoon and the underestimation of its intensity and to the northern shift of the West African Heat Low (Panitz et al., 2014), errors in the simulation of the lateral terrestrial water flow and its contribution to land surface evaporation(Arnault et al., 2021), as well as underestimation of the surface short-wave radiation and

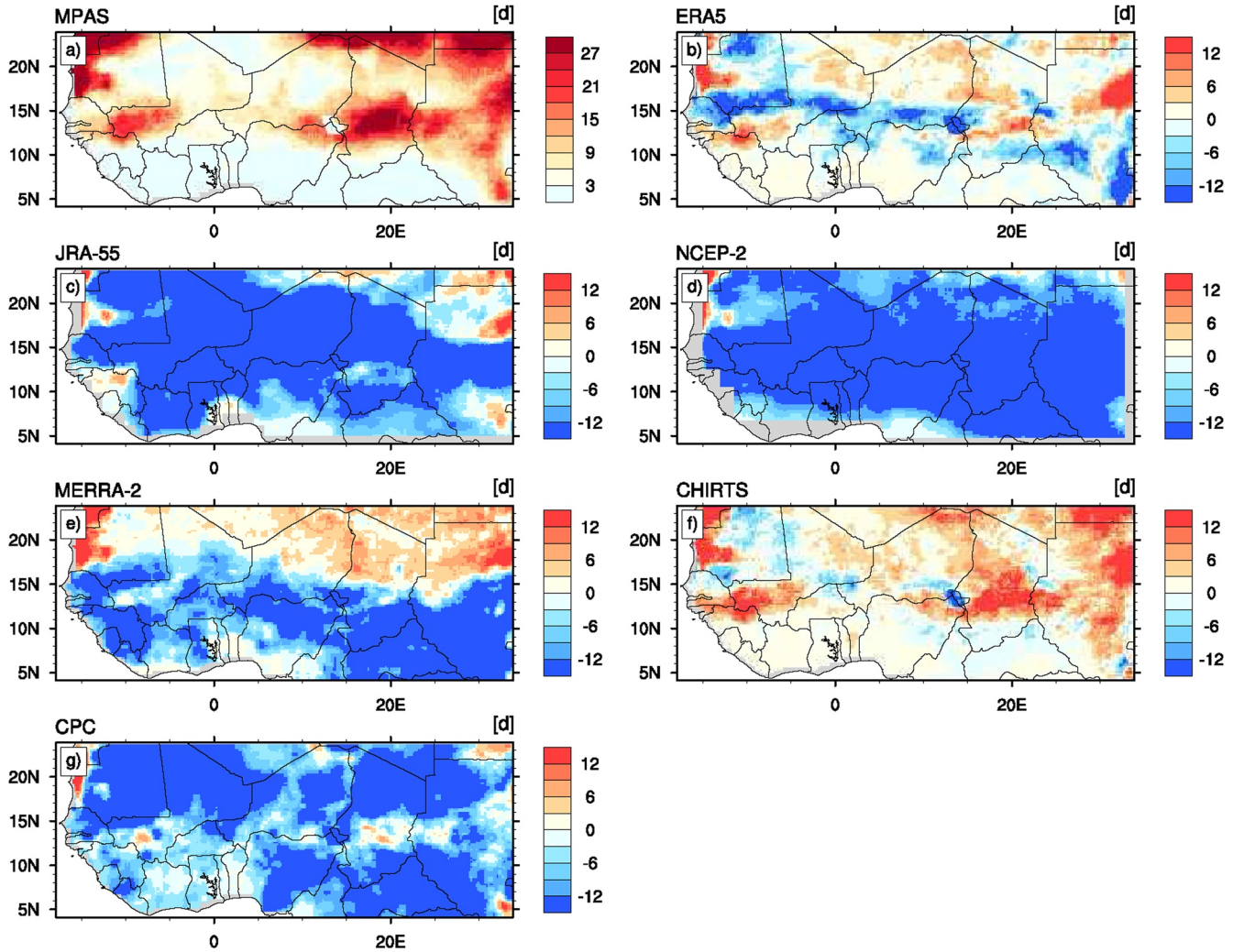

Figure 10. As in Figure 8 but for the heat wave duration index HWDI.

latent heat flux, cloudiness, surface water and the surface albedo (Diallo et al., 2017; Dieng et al., 2017; Sylla et al., 2009). In applications of the WRF model together with the Noah-LSM, Glotfelty et al. (2021) identified the satellite derived albedo climatology as a source of additional errors. Careto et al. (2018) linked higher temperatures to evaporative stress and strong soil moisture temperature coupling in some areas. For the Sahel, however, they stated that precipitation regimes are more important. Finally, as pointed out by Heinzeller et al. (2018), the choice of physical parametrizations can greatly influence the model's capabilities, especially the accuracy of the surface temperature and precipitation.

On the other hand, a further analysis to understanding the mechanism responsible for model's deficiencies in simulating mean atmospheric variables over West Africa may not necessarily explain the biases in the extreme values because of the weak synoptic circulation and forcing over the region. The extreme values are not reached at the same time over all the grid points in the region. This makes it difficult to isolate the atmospheric conditions which induce extremes over the region. Such analysis would require application of Self-Organizing Maps to first group areas that experience extreme events at the same time and analyze the atmospheric feature responsible for each group as done in Abiodun et al. (2016) and Abatan et al. (2023). However, such analysis is beyond the scope of the present study, but it is be a focus of our future studies.

With reference to ERA5, MPAS gives a credible simulation of mean temperature and wind patterns over West Africa (Figure 13). It captures all essential features in the temperature field. The features include the zonal distribution of the temperature pattern, the Sahel-heat-load induced temperature maxima (in the west Sahel), the

Table 5
Mean Values of Precipitation Indices Over the Investigation Areas for the JJA Season, Both Observed and Simulated

Area	Data	RR (mm/d)	RR1 (d)	RX1day (mm/d)
SAH_W	S	3.7–4.6–7.0	32.8–39.3–47.6	22.0–41.3–68.1
	G	3.9–4.3–4.6	33.8–40.3–49.6	29.1–39.3–46.2
	R	2.8–4.1–5.2	23.8–47.2–63.6	25.7–33.5–43.1
	MPAS_A	2.7	41.3	23.5
	MPAS_B	2.8	42.1	24.1
	MPAS	2.8	41.7	23.8
SAH_E	S	2.1–2.9–4.7	22.1–29.5–37.5	18.2–29.8–51.5
	G	2.5–2.8–3.1	25.9–31.2–38.8	23.3–31.0–40.5
	R	2.4–3.1–3.7	25.9–41.5–49.1	16.7–28.1–44.1
	MPAS_A	2.9	40.0	21.3
	MPAS_B	2.6	38.1	20.8
	MPAS	2.8	39.1	21.1

Note. S, G, and R denote minimum, mean and maximum values of observational datasets for satellite (S), gauge (G), and reanalysis (R) products as presented by Dosio et al. (2021b).

topographically induced temperature minima (i.e., over Jos Plateau, Guinean Highlands and Mount Cameroon), and the monsoon wind system, which consists of south-westerly and north-easterly flows and their associated line of Intercontinental Discontinuity (ITD; Nicholson, 2013; Redelsperger et al., 2006). Nevertheless, there are substantial cold biases in the temperature field (up about 3°C over the Sahel region). The cold bias can be attributed to several factors. For instance, it could be due to deficiencies in radiation parameterization routines (e.g., too much aerosol particles in the model (Fabien et al., 2012; Huang et al., 2019) or shortcomings in the land parameterization scheme (e.g., inappropriate land cover types (Domínguez et al., 2010);). However, the cold biases reduces the simulated ocean-land temperature gradient, southwest monsoon flow (Figure 13c) and inland transport of moisture form the ocean.

In summary, it can be stated that the MPAS global static 60-km mesh approach does not provide higher fidelity than the regional climate models. However, the ability of MPAS to apply variable meshes in a regional refinement and to run in convection permitting mode opens possibilities for improvements, as shown by Heinzeller et al. (2016). Also, the results obtained from the two procedures employed for initializing the model, MPAS_A and MPAS_B, are very similar. Table 6 shows very similar mean values and standard deviations for the applied statistics.However, the long-term run of MPAS_B appears to exhibit higher standard deviations in many variables.

Similar results are obtained when the entire area from −18° to 35° longitude and from 4° to 24° latitude (Figure 2) is considered. Table 7 shows the parameters of the distributions of the MPAS_A and MPAS_B experiments

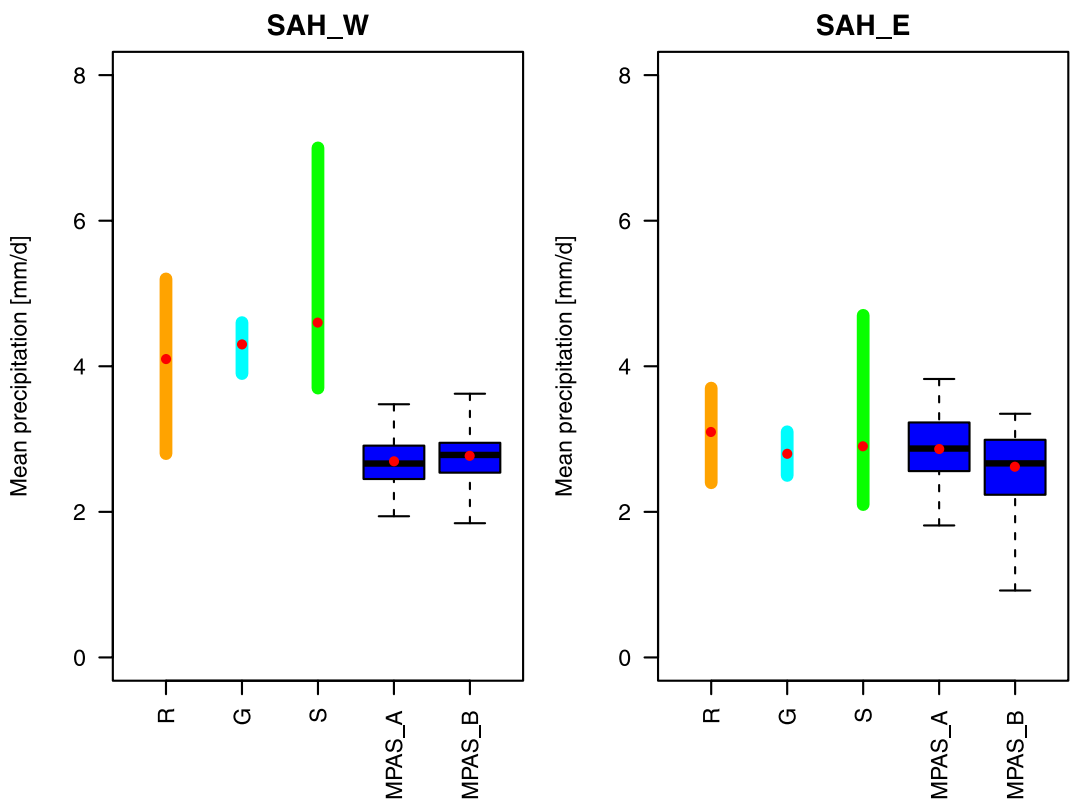

Figure 11. Boxplots of the simulated daily mean precipitation RR and ranges of observational datasets for satellite (S), gauge (G), and reanalysis (R) products as presented by Dosio et al. (2021b) in the investigation areas SAH_W and SAH_E and the summer season (JJA).

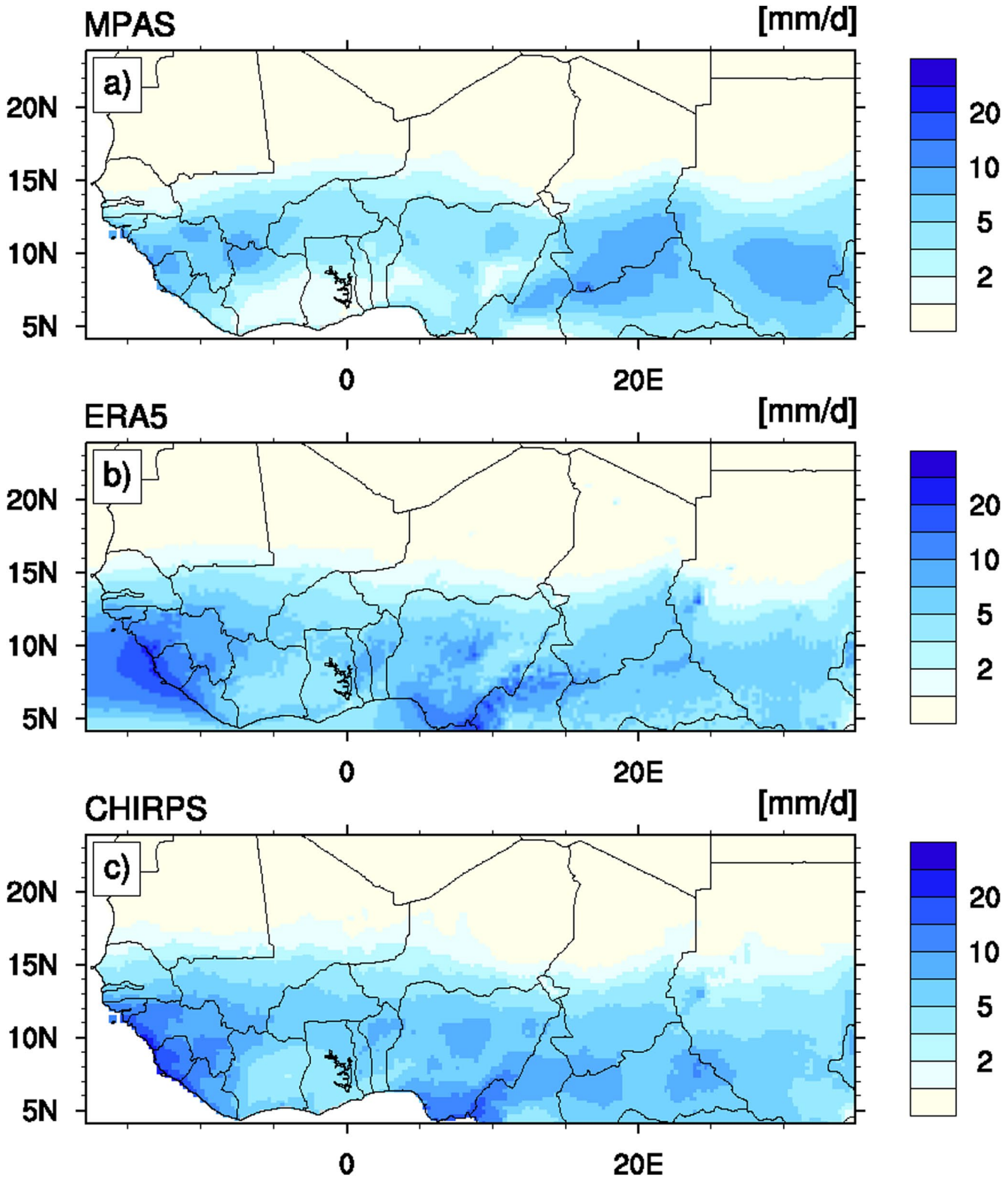

Figure 12. Mean summer (JJA) precipitation as in (a) average of the MPAS simulations, (b) ERA5 reanalysis, and (c) CHIRPS observations.

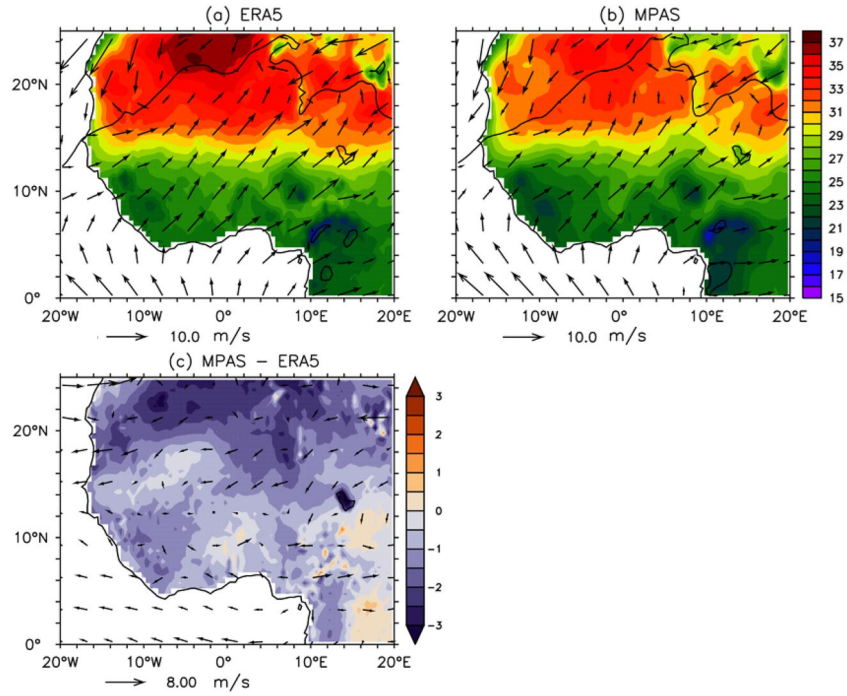

Figure 13. June–July–August (JJA) mean temperature in °C and 850 mb wind (arrows) in m/s for (a) ERAS, (b) MPAS, and (c) MPAS biases (MPAS–ERA5) in the period 1981–2010. The thick black line in panel (a) and (b) indicates the line of Intercontinental Discontinuity (ITD).

for the investigated indices in this area. The results show only small differences in the mean values. Compared to MPAS_A, MPAS_B reveals slightly larger standard deviations. Also, the ranges are marginally larger. In the majority of the cases this is due to a smaller minimum value. These results demonstrate that the different approaches to the model initialization are principally equivalent. However, a careful selection of specific years in the approach MPAS_A is needed.

4. Conclusions

A large ensemble of 51 simulations with the Model for Prediction Across Scales (MPAS) has been used to assess its ability to reproduce the summer (JJA) extreme temperature and heat waves in the area of West Africa. With its global approach, the model avoids transition errors influencing the performance of limited area climate models.

Table 6
Mean Value and Standard Deviations of the Applied Statists and the Different Initalizations as in MPAS_A and MPAS_B, Units Are °C for TG, TX, TXx, Day for TR, SU, RR1, and mm/day for RR and RX1day

	SAH_W				SAH_E				GUI_C			
	MPAS-A		MPAS-B		MPAS-A		MPAS-B		MPAS-A		MPAS-B	
Index	Mean	SD	Mean	SD	Mean	SD	Mean	SD	Mean	SD	Mean	SD
TG	28.8	0.27	28.5	0.28	28.8	0.37	28.8	0.37	24.1	0.22	24.1	0.26
TX	33.1	0.36	32.7	0.46	33.2	0.53	32.8	0.58	27.4	0.28	26.8	0.37
TXx	38.5	0.74	38.6	0.52	38.7	0.79	38.3	0.6	30.6	0.45	30.1	0.57
TR	52.3	3.15	49.5	3.81	51.8	3.46	56.4	4.42	3.1.	1.19	2.0	1.24
SU	33.6	2.99	31.7	3.51	33.6	3.94	29.7	4.69	0.	–	0.	–
RR	2.7	0.36	2.8	0.40	2.9.	0.48	2.6	0.57	3.3	0.34	3.4	0.47
RR1	41.3	3.16	42.1	3.99	40.0	3.59	38.1	4.36	57.9	4.38	60.2	6.43
RX1day	23.5	6.97	24.1	8.33	21.3	5.99	20.8	7.62	18.8	2.16	17.6	1.77

Table 7
Minimum, Mean, Maximum Values, and Standard Deviations of the Applied Statists and the Different Initalizations as in the Entire Investigated West African and Sahel Zone as in Figure 2

	MPAS_A				MPAS_A			
Index	Minimum	Mean	Maximum	SD	Minmum	Mean	Maxmum	SDS
TG	27.9	28.4	28.9	0.25	27.9	28.3	28.8	0.27
TX	32.8	33.3	34.0	0.28	32.2	32.8	33.7	0.38
TXx	36.8	38.0	39.0	0.58	36.7	37.4	38.1	0.39
TR	33.3	38.3	42.7	2.45	34.4	41.4	47.6	3.82
SU	36.0	39.1	43.6	1.77	31.5	35.6	41.5	2.41
RR	2.1	2.4	2.8	0.18	1.9	2.4	2.9	0.21
RR1	33.6	35.8	39.5	1.37	33.6	36.3	42.2	2.01
RX1day	10.6	15.6	22.3	2.84	8.9	15.5	21.8	3.84

Note. Units are °C for TG, TX, TXx, day for TR, SU, RR1, and mm/d for RR and RX1day.

Also, the simulations are not confined by a driving model. The MPAS simulations were driven by the SST and sea ice extent as the only boundary conditions.

The results reveal moderate cold biases in the range from −0.6° to −0.9°C for the daily mean temperature and increase to −1.2° to −2.0°C for the area mean of the daily maximum temperature TX and to −2.2° to −2.7°C for TXx as the maximum of TX. The bias in the number of tropical nights TN ranges from +3 to −10 days. An underestimation by up to 50% is also present in the number of summer days SU with TX > 35°C. The percentage of days when TN > the 90th percentile TN90p as well as the percentage of days when TX > the 90th percentile TX90p reveal underestimations by up to 50%, and the heat wave duration index HWDI is underestimated by 10%–60%. Compared to the reanalyses, the biases revealed by the MPAS simulations are generally smaller than with the measured observational reference. Because of the present and reported deficiencies in the observed data for the Sahel, the shortcomings in the MPAS simulations are in reality most likely smaller.

Regional biases are to a large extent negative. Regarding temperatures, the smallest biases occur in West Africa. The smallest biases in precipitation occur in the eastern part. However, the underestimation in the first case and the overestimation in the second reveal that improvements of the model regarding its physics, land–surface scheme, and land surface input data are required for an adequate simulation of the WA and Sahelian climate.

The results obtained from the two model initialization procedures used are very similar and demonstrate the equivalence of the two approaches. Compared to long term runs, selections of the initialization years in relation to the spread of mean SST temperatures in the Gulf of Guinea extremely reduce the demand on the CPU, especially when only short terms, such as months or specific seasons, are considered.

Shortcomings in the reproduction of temperatures and precipitation found in the present investigation indicate that the global approach per se does not provide higher fidelity than the regional climate models. Kim et al. (2014) showed that in CORDEX-Africa, multi model ensembles generally outperformed the single ensembles. In such ensemble approaches, MPAS simulations can be applied as an adequate member.

Data Availability Statement

The data generated for this study has been made available at the osf.io/36ebd repository. The required calculations were performed and figures created by employing the CDO (Schulzweida, 2021), NCO (Zender, 2022), R (R Core Team, 2021), and NCL (NCL, 2021) software packages.

Acknowledgments
The authors thank the University of Cape Town, South Africa, for providing access to the UCT HPC facility. The study was funded by the German Federal Ministry of Science and Education (BMBF) within the Doctorate Research Programme of West African Science Service Centre on Climate Change and Adapted Land Use (WASCAL-DRP-WACS), whose support is gratefully acknowledged. Open Access funding enabled and organized by Projekt DEAL.

References

Abatan, A., Collins, M., Babel, M., Khadka, D., & De Silva, Y. (2023). Sub-seasonal to seasonal drivers of dry extreme rainfall events over Northeast Thailand. *Frontiers in Climate*, *4*, 1031226. https://doi.org/10.3389/fclim.2022.1031226

Abiodun, B., Abba Omar, S., Lennard, C., & Jack, C. (2016). Using regional climate models to simulate extreme rainfall events in the Western Cape, South Africa. *International Journal of Climatology*, *36*(2), 689–705. https://doi.org/10.1002/joc.4376

Adeniyi, M., & Oyekola, S. (2017). Assessment of heat and cold wave events over West Africa using three regional climate models. *Annales Geophysicae*, *60*(3), A0322. https://doi.org/10.4401/ag-7039

Ahmed, K., Wang, G., Yu, M., Koo, J., & You, L. (2015). Potential impact of climate change on cereal crop yield in West Africa. *Climatic Change*, *133*(2), 321–334. https://doi.org/10.1007/s10584-015-1462-7

Arnault, J., Fersch, B., Rummler, T., Zhang, Z., Quenum, G. M., Wei, J., et al. (2021). Lateral terrestrial water flow contribution to summer precipitation at continental scale—a comparison between Europe and West Africa with WRF-Hydro-tag ensembles. *Hydrological Processes*, *35*(5), e14183. https://doi.org/10.1002/hyp.14183

Arnault, J., Knoche, R., Wei, J., & Kunstmann, H. (2016). Evaporation tagging and atmospheric water budget analysis with WRF: A regional precipitation recycling study for West Africa. *Water Resources Research*, *52*(3), 1544–1567. https://doi.org/10.1002/2015WR017704

Broxton, P. D., Zeng, X., Sulla-Menashe, D., & Troch, P. A. (2014). A MODIS-based global 1-km maximum green vegetation fraction dataset. *Journal of Applied Meteorology and Climatology*, *53*(6), 1593–1605. https://doi.org/10.1175/JAMC-D-13-0270.1

Careto, J. A. M., Cardoso, R. M., Soares, P. M. M., & Trigo, R. M. (2018). Land-atmosphere coupling in CORDEX-africa: Hindcast regional climate simulations. *Journal of Geophysical Research: Atmospheres*, *123*(19), 11048–11067. https://doi.org/10.1029/2018JD028378

Chen, F., Mitchell, K., Schaake, J., Xue, Y., Pan, H., Koren, V., et al. (1996). Modeling of land-surface evaporation by four schemes and comparison with FIFE observations. *Journal of Geophysical Research*, *101*(D3), 7251–7268. https://doi.org/10.1029/95JD02165

Clough, S., Shephard, M., Mlawer, E., Delamere, J., Iacono, M., Cady-Pereira, K., et al. (2005). Atmospheric radiative transfer modeling: A summary of the AER codes. *Journal of Quantitative Spectroscopy and Radiative Transfer*, *91*(2), 233–244. https://doi.org/10.1016/j.jqsrt.2004.05.058

Cook, K. H. (2008). The mysteries of Sahel droughts. *Nature Geoscience*, *1*(10), 647–648. https://doi.org/10.1038/ngeo320

Coumou, D., & Rahmstorf, S. (2012). A decade of weather extremes. *Nature Climate Change*, *2*(7), 491–496. https://doi.org/10.1038/nclimate1452

Danielson, J. J., & Gesch, D. B. (2011). Global multi-resolution terrain elevation data 2010 (GMTED2010) (USGS Numbered Series No. 2011-1073). *Earth Resources Observation and Science (EROS) Center*. https://doi.org/10.3133/ofr20111073

Dee, D. P., Uppala, S. M., Simmons, A. J., Berrisford, P., Poli, P., Kobayashi, S., et al. (2011). The ERA-interim reanalysis: Configuration and performance of the data assimilation system. *Quarterly Journal of the Royal Meteorological Society*, *137*(656), 553–597. https://doi.org/10.1002/qj.828

Diallo, F. B., Hourdin, F., Rio, C., Traore, A.-K., Mellul, L., Guichard, F., & Kergoat, L. (2017). The surface energy budget computed at the grid-scale of a climate model challenged by station data in West Africa. *Journal of Advances in Modeling Earth Systems*, *9*(7), 2710–2738. https://doi.org/10.1002/2017MS001081

Dieng, D., Smiatek, G., Bliefernicht, J., Heinzeller, D., Sarr, A., Gaye, A. T., & Kunstmann, H. (2017). Evaluation of the COSMO-CLM high-resolution climate simulations over West Africa. *Journal of Geophysical Research: Atmospheres*, *122*(3), 1437–1455. https://doi.org/10.1002/2016JD025457

Dilley, M., & Heyman, B. N. (1995). ENSO and disaster: Droughts, floods and El Niño/southern oscillation warm events. *Disasters*, *19*(3), 181–193. https://doi.org/10.1111/j.1467-7717.1995.tb00338.x

Domínguez, M., Gaertner, M. A., de Rosnay, P., & Losada, T. (2010). A regional climate model simulation over West Africa: Parameterization tests and analysis of land-surface fields. *Climate Dynamics*, *35*(1), 249–265. https://doi.org/10.1007/s00382-010-0769-3

Dosio, A. (2016). Projections of climate change indices of temperature and precipitation from an ensemble of bias-adjusted high-resolution EURO-CORDEX regional climate models. *Journal of Geophysical Research: Atmospheres*, *121*(10), 5488–5511. https://doi.org/10.1002/2015JD024411

Dosio, A. (2017). Projection of temperature and heat waves for Africa with an ensemble of CORDEX regional climate models. *Climate Dynamics*, *49*(1–2), 493–519. https://doi.org/10.1007/s00382-016-3355-5

Dosio, A., Jury, M., Almazroui, M., Ashfaq, M., Diallo, I., Engelbrecht, F. A., et al. (2021a). Projected future daily characteristics of African precipitation based on global (CMIP5, CMIP6) and regional (CORDEX, CORDEX-CORE) climate models. *Climate Dynamics*, *57*(11–12), 3135–3158. https://doi.org/10.1007/s00382-021-05859-w

Dosio, A., Lennard, C., & Spinoni, J. (2022). Projections of indices of daily temperature and precipitation based on bias-adjusted CORDEX-Africa regional climate model simulations. *Climatic Change*, *170*(1), 13. https://doi.org/10.1007/s10584-022-03307-0

Dosio, A., Panitz, H.-J., Schubert-Frisius, M., & Lühi, D. (2015). Dynamical downscaling of CMIP5 global circulation models over CORDEX-Africa with COSMO-CLM: Evaluation over the present climate and analysis of the added value. *Climate Dynamics*, *44*(9), 2637–2661. https://doi.org/10.1007/s00382-014-2262-x

Dosio, A., Pinto, I., Lennard, C., Sylla, M. B., Jack, C., & Nikulin, G. (2021b). What can we know about recent past precipitation over Africa? Daily characteristics of African precipitation from a large ensemble of observational products for model evaluation. *Earth and Space Science*, *8*(10), e2020EA001466. https://doi.org/10.1029/2020EA001466

Engdaw, M. M., Ballinger, A. P., Hegerl, G. C., & Steiner, A. K. (2022). Changes in temperature and heat waves over Africa using observational and reanalysis data sets. *International Journal of Climatology*, *42*(2), 1165–1180. https://doi.org/10.1002/joc.7295

Fabien, S., Elguindi, N., & Mallet, M. (2012). Radiative and climatic effects of dust over West Africa, as simulated by a regional climate model. *Climate Research*, *52*, 97–113. https://doi.org/10.3354/cr01039

Funk, C., Peterson, P., Landsfeld, M., Pedreros, D., Verdin, J., Shukla, S., et al. (2015). The climate hazards infrared precipitation with stations—A new environmental record for monitoring extremes. *Scientific Data*, *2*(1), 150066. https://doi.org/10.1038/sdata.2015.66

Funk, C., Peterson, P., Peterson, S., Shukla, S., Davenport, J. F., MichaelsenKnapp, K. R., et al. (2019). A high-resolution 1983–2016 T_{max} climate data record based on infrared temperatures and stations by the climate hazard center. *Journal of Climate*, *32*(17), 5639–5658. https://doi.org/10.1175/jcli-d-18-0698.1

Gbobaniyi, E., Sarr, A., Sylla, M. B., Diallo, I., Lennard, C., Dosio, A., et al. (2014). Climatology, annual cycle and interannual variability of precipitation and temperature in CORDEX simulations over West Africa. *International Journal of Climatology*, *34*(7), 2241–2257. https://doi.org/10.1002/joc.3834

Gelaro, R., McCarty, W., Suárez, M. J., Todling, R., Molod, A., Takacs, L., et al. (2017). The modern-era retrospective analysis for Research and applications, Version 2 (MERRA-2). *Journal of Climate*, *30*(14), 5419–5454. https://doi.org/10.1175/JCLI-D-16-0758.1

Glotfelty, T., Ramírez-Mejía, D., Bowden, J., Ghilardi, A., & West, J. J. (2021). Limitations of WRF land surface models for simulating land use and land cover change in Sub-Saharan Africa and development of an improved model (CLM-AF v. 1.0). *Geoscientific Model Development*, *14*(6), 3215–3249. https://doi.org/10.5194/gmd-14-3215-2021

Grist, J. P., & Nicholson, S. E. (2001). A study of the dynamic factors influencing the rainfall variability in the West African Sahel. *Journal of Climate*, *14*(7), 1337–1359. https://doi.org/10.1175/1520-0442(2001)014⟨1337:ASOTDF⟩2.0.CO;2

Haile, M. (2005). Weather patterns, food security and humanitarian response in sub-Saharan Africa. *Philosophical Transactions of the Royal Society B: Biological Sciences*, *360*(1463), 2169–2182. https://doi.org/10.1098/rstb.2005.1746

Harris, I., Osborn, T. J., Jones, P., & Lister, D. (2020). Version 4 of the CRU TS monthly high-resolution gridded multivariate climate dataset. *Scientific Data*, *7*(1), 109. https://doi.org/10.1038/s41597-020-0453-3

Heinzeller, D., Dieng, D., Smiatek, G., Olusegun, C., Klein, C., Hamann, I., et al. (2018). The WASCAL high-resolution regional climate simulation ensemble for West Africa: Concept, dissemination and assessment. *Earth System Science Data*, *10*(2), 815–835. https://doi.org/10.5194/essd-10-815-2018

Heinzeller, D., Duda, M. G., & Kunstmann, H. (2016). Towards convection-resolving, global atmospheric simulations with the model for prediction across scales (MPAS) v3.1: An extreme scaling experiment. *Geoscientific Model Development*, *9*(1), 77–110. https://doi.org/10.5194/gmd-9-77-2016

Hernández-Díaz, L., Laprise, R., Sushama, L., Martynov, A., Winger, K., & Dugas, B. (2013). Climate simulation over CORDEX africa domain using the fifth-generation Canadian regional climate model (CRCM5). *Climate Dynamics*, *40*(5), 1415–1433. https://doi.org/10.1007/s00382-012-1387-z

Hersbach, H., Bell, B., Berrisford, P., Hirahara, S., Horányi, A., Muñoz-Sabater, J., et al. (2020). The ERA5 global reanalysis. *Quarterly Journal of the Royal Meteorological Society*, *146*(730), 1999–2049. https://doi.org/10.1002/qj.3803

Huang, H., Gu, Y., Xue, Y., Jiang, J., & Zhao, B. (2019). Assessing aerosol indirect effect on clouds and regional climate of East/South Asia and West Africa using NCEP GFS. *Climate Dynamics*, *52*(9–10), 5759–5774. https://doi.org/10.1007/s00382-018-4476-9

Janicot, S., Moron, V., & Fontaine, B. (1996). Sahel droughts and ENSO dynamics. *Geophysical Research Letters*, *23*(5), 515–518. https://doi.org/10.1029/96GL00246

Kanamitsu, M., Ebisuzaki, W., Woollen, J., Yang, S.-K., Hnilo, J. J., Fiorino, M., & Potter, G. L. (2002). NCEP–DOE AMIP-II reanalysis (R-2). *Bulletin of the American Meteorological Society*, *83*(11), 1631–1644. https://doi.org/10.1175/BAMS-83-11-1631

Karl, T., Nicholls, N., & Ghazi, A. (1999). Workshop summary Weather and Climate Extremes. In T. Karl, N. Nicholls, & A. Ghazi (Eds.), *CLIVAR/GCOS/WMO workshop on indices and indicators for climate extremes* (pp. 3–7). Springer. https://doi.org/10.1007/978-94-015-9265-9_2

Kim, J., Waliser, D. E., Mattmann, C. A., Goodale, C. E., Hart, A. F., Zimdars, P. A., et al. (2014). Evaluation of the CORDEX-africa multi-RCM hindcast: Systematic model errors. *Climate Dynamics*, *42*(5), 1189–1202. https://doi.org/10.1007/s00382-013-1751-7

Klemp, J. B. (2011). A terrain-following coordinate with smoothed coordinate surfaces. *Monthly Weather Review*, *139*(7), 2163–2169. https://doi.org/10.1175/MWR-D-10-05046.1

Kobayashi, C., & Iwasaki, T. (2016). Brewer-Dobson circulation diagnosed from JRA-55. *Journal of Geophysical Research: Atmospheres*, *121*(4), 1493–1510. https://doi.org/10.1002/2015JD023476

Lobell, D. B., Schlenker, W., & Costa-Roberts, J. (2011). Climate trends and global crop production since 1980. *Science*, *333*(6042), 616–620. https://doi.org/10.1126/science.1204531

Maoyi, M. L., & Abiodun, B. J. (2021). How well does MPAS-atmosphere simulate the characteristics of the Botswana High? *Climate Dynamics*, *57*(7–8), 2109–2128. https://doi.org/10.1007/s00382-021-05797-7

Masunaga, H., Schröder, M., Furuzawa, F. A., Kummerow, C., Rustemeier, E., & Schneider, U. (2019). Inter-product biases in global precipitation extremes. *Environmental Research Letters*, *14*(12), 125016. https://doi.org/10.1088/1748-9326/ab5da9

NCL. (2021). The NCAR Command Language. version 6.6.2 [Software]. UCAR/NCAR/CISL/TDD. https://doi.org/10.5065/D6WD3XH5

New, M., Hewitson, B., Stephenson, D. B., Tsiga, A., Kruger, A., Manhique, A., et al. (2006). Evidence of trends in daily climate extremes over southern and west Africa. *Journal of Geophysical Research*, *111*(D14). https://doi.org/10.1029/2005JD006289

Nicholson, S. E. (2013). The West African Sahel: A review of recent studies on the rainfall regime and its interannual variability. *International Scholarly Research Notices*, *32*, 1–32. https://doi.org/10.1155/2013/453521

Nicholson, S. E., & Webster, P. J. (2007). A physical basis for the interannual variability of rainfall in the Sahel. *Quarterly Journal of the Royal Meteorological Society*, *133*(629), 2065–2084. https://doi.org/10.1002/qj.104

Nikiema, P. M., Sylla, M. B., Ogunjobi, K., Kebe, I., Gibba, P., & Giorgi, F. (2017). Multi-model CMIP5 and CORDEX simulations of historical summer temperature and precipitation variabilities over West Africa. *International Journal of Climatology*, *37*(5), 2438–2450. https://doi.org/10.1002/joc.4856

Omotosho, J. B., & Abiodun, B. J. (2007). A numerical study of moisture build-up and rainfall over west africa. *Meteorological Applications*, *14*(3), 209–225. https://doi.org/10.1002/met.11

Oueslati, B., Pohl, B., Moron, V., Rome, S., & Janicot, S. (2017). Characterization of heat waves in the Sahel and associated physical mechanisms. *Journal of Climate*, *30*(9), 3095–3115. https://doi.org/10.1175/JCLI-D-16-0432.1

Panitz, H.-J., Dosio, A., Büchner, M., Lüthi, D., & Keuler, K. (2014). COSMO-CLM (CCLM) climate simulations over CORDEX- africa domain: Analysis of the ERA-Interim driven simulations at 0.44°and 0.22° resolution. *Climate Dynamics*, *42*(11–12), 3015–3038. https://doi.org/10.1007/s00382-013-1834-5

Perkins, D. M., Bailey, R. A., Dossena, M., Gamfeldt, L., Reiss, J., Trimmer, M., & Woodward, G. (2015). Higher biodiversity is required to sustain multiple ecosystem processes across temperature regimes. *Global Change Biology*, *21*(1), 396–406. https://doi.org/10.1111/gcb.12688

Poan, E. D., Gachon, P., Dueymes, G., Diaconescu, E., Laprise, R., & Seidou Sanda, I. (2016). West African monsoon intraseasonal activity and its daily precipitation indices in regional climate models: Diagnostics and challenges. *Climate Dynamics*, *47*(9), 3113–3140. https://doi.org/10.1007/s00382-016-3016-8

R Core Team. (2021). R: A language and environment for statistical computing. Retrieved from https://www.R-project.org/

Redelsperger, J.-L., Thorncroft, C. D., Diedhiou, A., Lebel, T., Parker, D. J., & Polcher, J. (2006). African monsoon multidisciplinary analysis: An international research project and field campaign. *Bulletin of the American Meteorological Society*, *87*(12), 1739–1746. https://doi.org/10.1175/BAMS-87-12-1739

Ringard, J., Dieppois, B., Rome, S., Diedhiou, A., Pellarin, T., Konaré, A., et al. (2016). The intensification of thermal extremes in west Africa. *Global and Planetary Change*, *139*, 66–77. https://doi.org/10.1016/j.gloplacha.2015.12.009

Ringler, T., Thuburn, J., Klemp, J., & Skamarock, W. (2010). A unified approach to energy conservation and potential vorticity dynamics for arbitrarily-structured C-grids. *Journal of Computational Physics*, *229*(9), 3065–3090. https://doi.org/10.1016/j.jcp.2009.12.007

Russo, S., Marchese, A. F., Sillmann, J., & Immé, G. (2016). When will unusual heat waves become normal in a warming Africa? *Environmental Research Letters*, *11*(5), 054016. https://doi.org/10.1088/1748-9326/11/5/054016

Saha, S., Moorthi, S., Wu, X., Wang, J., Nadiga, S., Tripp, P., et al. (2014). The NCEP climate Forecast system version 2. *Journal of Climate*, *27*(6), 2185–2208. https://doi.org/10.1175/JCLI-D-12-00823.1

Schulzweida, U. (2021). CDO user guide. Version 2.0.0. https://doi.org/10.5281/zenodo.5614769

Sivakumar, M., Collins, C., Jay, A., & Hansen, J. (2014). *Regional priorities for strenghtening climate services for farmers in Africa and South Asia (CCAFS Working Paper No. 71). CGIAR Research Program on Climate Change*. Agriculture and Food Security (CCAFS).

Skamarock, W. C., Klemp, J. B., Duda, M. G., Fowler, L. D., Park, S., & Ringler, D. T. (2012). A multiscale nonhydrostatic atmospheric model using centroidal Voronoi tesselations and C-grid staggering. *Monthly Weather Review*, *140*(9), 3090–3105. https://doi.org/10.1175/mwr-d-11-00215.1

Smiatek, G., & Kunstmann, H. (2023). Potential impact of the pan-african great green wall on Sahelian summer precipitation: A global modeling approach with MPAS. *Earth Interactions*, *27*(1), 220013. https://doi.org/10.1175/EI-D-22-0013.1

Son, J.-H., & Seo, K.-H. (2020). Mechanisms for the climatological characteristics and interannual variations of the Guinea coast precipitation: Early summer West African monsoon. *Atmosphere*, *11*(4), 396. https://doi.org/10.3390/atmos11040396

Sultan, B., Roudier, P., Quirion, P., Alhassane, A., Muller, B., Dingkuhn, M., et al. (2013). Assessing climate change impacts on sorghum and millet yields in the Sudanian and Sahelian savannas of West Africa. *Environmental Research Letters*, *8*(1), 014040. https://doi.org/10.1088/1748-9326/8/1/014040

Sylla, M. B., Gaye, A. T., Pal, J. S., Jenkins, G. S., & Bi, X. Q. (2009). High-resolution simulations of West African climate using regional climate model (RegCM3) with different lateral boundary conditions. *Theoretical and Applied Climatology*, *98*(3–4), 293–314. https://doi.org/10.1007/s00704-009-0110-4

Thuburn, J., Ringler, T., Skamarock, W., & Klemp, J. (2009). Numerical representation of geostrophic modes on arbitrarily structured C-grids. *Journal of Computational Physics*, *228*(22), 8321–8335. https://doi.org/10.1016/j.jcp.2009.08.006

Zender, C. (2022). *NCO user guide*. Department of Earth System Science, University of California.